



HAL
open science

Modeling, design, fabrication and experimentation of a GaN-based, ^{63}Ni betavoltaic battery

C Munson, Q. Gaimard, Kamel Merghem, S. Sundaram, J. Rogers, Jacques Sanoit (de), P Voss, A. Ramdane, Jean-Paul Salvestrini, A. Ougazzaden

► **To cite this version:**

C Munson, Q. Gaimard, Kamel Merghem, S. Sundaram, J. Rogers, et al.. Modeling, design, fabrication and experimentation of a GaN-based, ^{63}Ni betavoltaic battery. *Journal of Physics D: Applied Physics*, 2018, 51 (3), pp.035101. 10.1088/1361-6463/aa9e41 . cea-01765048

HAL Id: cea-01765048

<https://cea.hal.science/cea-01765048v1>

Submitted on 10 Jan 2019

HAL is a multi-disciplinary open access archive for the deposit and dissemination of scientific research documents, whether they are published or not. The documents may come from teaching and research institutions in France or abroad, or from public or private research centers.

L'archive ouverte pluridisciplinaire **HAL**, est destinée au dépôt et à la diffusion de documents scientifiques de niveau recherche, publiés ou non, émanant des établissements d'enseignement et de recherche français ou étrangers, des laboratoires publics ou privés.

Modeling, design, fabrication and experimentation of a GaN-based, ^{63}Ni betavoltaic battery

C E Munson IV^{1,2}, Q Gaimard³, K Merghem³, S Sundaram¹, D J Rogers⁴,
J de Sanoit⁵, P L Voss^{1,2}, A Ramdane³, J P Salvestrini^{1,2} 
and A Ougazzaden^{1,2}

¹ Georgia Tech Lorraine and CNRS, UMI GT-CNRS 2958, 2 rue Marconi, 57070 Metz, France

² Georgia Institute of Technology, School of ECE, 777 Atlantic Drive NW, Atlanta, GA 30332, United States of America

³ CNRS, C2N, Route de Nozay, 91460, Marcoussis, France

⁴ Nanovation, 8 route de Chevreuse, Chateaufort, 78117, France

⁵ CEA, LIST, DRT / DM2I / LCD, Batiment 451, 91191 Gif sur Yvette, France

E-mail: abdallah.ougazzaden@georgiatech-metz.fr

Abstract

GaN is a durable, radiation hard and wide-bandgap semiconductor material, making it ideal for usage with betavoltaic batteries. This paper describes the design, fabrication and experimental testing of 1 cm^2 GaN-based betavoltaic batteries (that achieve an output power of 2.23 nW) along with a full model that accurately simulates the device performance which is the highest to date (to the best of our knowledge) for GaN-based devices with a ^{63}Ni source.

Keywords: betavoltaic, battery, GaN, ^{63}Ni

1. Introduction

Numerous fields require long-life power sources on the micro- or milliwatt scale. Although lithium-ion batteries currently respond to many of the requirements, the technology only has a functional lifespan on the order of a few years and such batteries require frequent recharging. When replacement/recharging is excessively expensive or impractical (such as in pacemakers, undersea sensing electronics and space applications), however, another option is required and betavoltaic batteries (which convert beta particle energy into electricity by means of radiation-resistant p-n junctions) have long been considered an attractive option in that they do not need recharging and they have a lifespan in excess of a few decades. Unfortunately, however, practical fabrication of betavoltaics with adequate power outputs has proven difficult up till now.

Tritium (^3H), ^{63}Ni and ^{147}Pm are the most common radionuclei considered for use as sources in betavoltaic batteries. They offer (respectively) average beta particle energies of 5.6,

17.4 and 224.1 keV and half-lives of 12.3, 100 and 2.6 years [1]. The relatively low beta particle energies released from ^3H and ^{63}Ni , in particular, make them more suitable for use in consumer-grade batteries than ^{147}Pm since the beta particles can be selectively blocked by only a few micrometers of shielding and they can thus be safely and easily packaged. Amongst these two radionuclei, ^{63}Ni has a superior half-life, which makes it a better choice as a long-term energy source and it is, therefore, the source considered in this paper.

Previous studies on the conversion of ^{63}Ni beta particle energy into electricity by means of GaN-based p-n junctions reported output powers from 23 pW to 0.57 nW [2–5]. Note that, in practice, the power output is typically lower than theoretical expectations, which are often above 2 nW [6]. Similar experiments with silicon and SiC based devices using ^{63}Ni achieved output powers of around 15.4 pW [7] and 0.34 nW [8], though some silicon designs approached 9 nW [9].

In this paper, a new state-of-the-art betavoltaic consisting of a p-GaN / i-GaN / n-GaN PIN structure on top of which a thin

^{63}Ni layer is deposited, is fabricated and tested. Preliminary modeling for such a structure was introduced in a previous paper published by our group, along with a series and shunt resistance (SSR) model [10]. Similarly, there has also been MCNP-based simulations created to estimate the performance of ^{147}Pm sandwiched between p–n junction GaN layers [11].

In this paper, more refined versions of these models (for the ^{63}Ni betavoltaic absorption and electrical circuit) used to design the betavoltaic GaN PIN device along with its fabrication process, and the device performance, are presented. The establishment of a reusable betavoltaic cell test platform which was developed to conform with radiation safety norms is also reported.

2. Model

In the following, a ^{63}Ni absorption model is developed which takes into account both self-absorption and beta particle trajectory incidence angle. The SSR model for the PIN structure, (developed in previous work [10]) is also outlined.

2.1. ^{63}Ni absorption model

Monte Carlo (MC) simulations [1] were used to estimate the beta particle energy deposited into the GaN based on a fixed surface area (1 cm^2) of ^{63}Ni . The increase in activity and emitted power with ^{63}Ni thickness, was investigated in order to take into account the interplay of self-absorption, incidence angle and beta particle energy. A thickness range of 0 to 4000 nm was used for ^{63}Ni so that saturation effects could be studied for both thick and thin layers. The simulation results yield the proportion of emitted beta particle energy that makes it into the GaN material (denoted as $N(y, d, e, \theta)$, in nm). These are then be combined to form an overall ^{63}Ni model. This model considers reflectance from the device surface and all angles of incidence (equation 1), for an energy emittance profile mimicking that of ^{63}Ni (equation 2). It is also valid for various ^{63}Ni thicknesses as chosen by equation 3:

$$\alpha_\theta = \sum_{\theta=0}^{\pi} N(y, d, e, \theta) \times (1 - R_\theta) \times \Delta\theta \quad (1)$$

$$\alpha_e = \sum_{e=5\text{ keV}}^{60\text{ keV}} \alpha_\theta(y, d, e) \times Pr(E = e) \times \Delta e \quad (2)$$

$$\alpha_T(y, t) = \sum_{d=0}^t \alpha_e(y, d) \times \Delta d \quad (3)$$

where R_θ is the percent reflectance at a given angle θ , $Pr(E = e)$ is the probability of an electron being emitted from ^{63}Ni at the given energy e (eV), y is the y -coordinate of depth into the device (nm) and t is the total ^{63}Ni thickness (nm). Equation 4 provides an estimation for the total amount of energy P_{nm} emitted from a $1\text{ cm}^2 \times 1\text{ nm}$ volume of ^{63}Ni , not considering self-absorption (which is taken into account in the simulation data, N):

$$P_{\text{nm}} \sim \rho \times \frac{A}{10^7} \times E_{\text{avg}} \times q \quad \left(\frac{\text{W}}{\text{cm}^2 \times \text{nm}} \right) \quad (4)$$

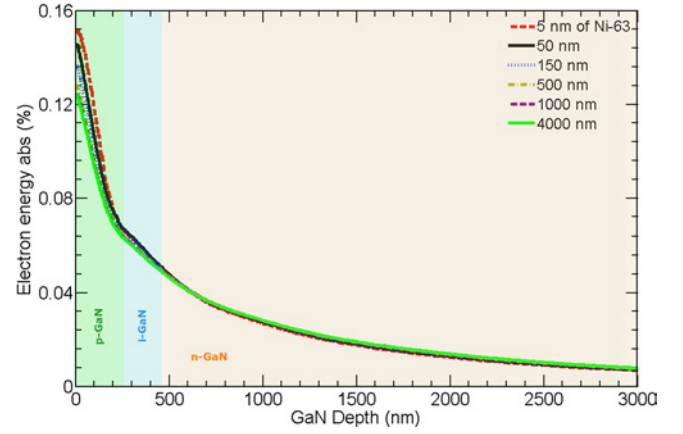


Figure 1. GaN beta particle absorption profiles for various ^{63}Ni thicknesses. ^{63}Ni layer not shown.

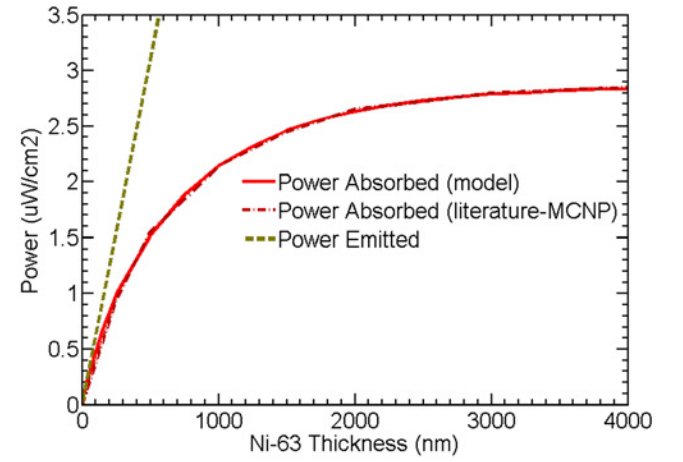


Figure 2. Power absorption efficiency in GaN versus ^{63}Ni thickness [12].

where ρ is the density of ^{63}Ni (8.91 g cm^{-3}) and A is the specific activity of ^{63}Ni per gram ($2.2 \times 10^{12}\text{ Bq/g}$) [4], E_{avg} is the average energy released from ^{63}Ni (17 keV) and q is the electron charge.

The results of these simulations, for a p-GaN / i-GaN / n-GaN PIN structure of 270 nm, 200 nm and $1\text{ }\mu\text{m}$, respectively, can be seen in figure 1, where we show the absorption profiles of beta particles in GaN for various ^{63}Ni thicknesses. For very thin layers of ^{63}Ni the GaN absorption is more pronounced, while for thick ^{63}Ni layers the profile smooths out to a more impeded, exponential absorption curve. This is possibly due to self-absorption as the ^{63}Ni source becomes thicker.

Finally, figure 2 shows that the power absorbed in the GaN material saturates towards $2.85\text{ }\mu\text{W cm}^{-2}$ as the ^{63}Ni thickness increases. Assuming an unlimited device size, the optimal ^{63}Ni thickness is infinitely thin, since this would result in the least amount of self-absorption. It can be estimated that the optimal ^{63}Ni thickness (for a 1 cm^2 sized device) is around 1500 nm of ^{63}Ni , since the absorbed power quickly begins to saturate after this point. These results match well with results published in literature, which demonstrate a similar saturation towards $2.85\text{ }\mu\text{W cm}^{-2}$ with increasing ^{63}Ni thickness [12].

2.2. Device model and series–shunt resistance model

The device modeling software used for this paper was Silvaco, although any device modeling software could be used. The SSR models were used in order to take into account the non-ideal behavior of the PIN diode and contacts, which consider both recombination effects and defects introduced by the device, as well as imperfections due to contacts. Taking into account these series and shunt resistances, which can be determined experimentally or estimated based on similar devices, the current and voltage of the PIN diode can be rewritten as:

$$V = I_d \times R_s + \left(1 + \frac{R_s}{R_{sh}}\right) \times V_d \quad (5)$$

$$I = I_d + \frac{V_d}{R_{sh}} \quad (6)$$

where R_s is the total series resistance, R_{sh} the total shunt resistance, and I_d and V_d are, respectively, the current and voltage obtained using a Silvaco simulation of the ideal PIN structure.

3. Design, material growth, processing and packaging

3.1. Device design

The device design was governed by the total amount of ^{63}Ni activity available. A device consisted of a p-GaN/i-GaN/n-GaN PIN structure on top of which a thin ^{63}Ni layer was placed. As it has been seen before, the optimal ^{63}Ni thickness, for a 1 cm^2 sized device, is around 1500 nm . This thickness corresponds to around 1.2 GBq of activity after electrodeposition (see subsection material growth). This means that six devices with 1 cm^2 in size could be realized. This number of devices is reasonable knowing that the final mounting of the devices will be done in a sealed glovebox leading to a non-negligible risk of having failed devices at the end (see subsection packaging).

Considering a realistic p-type doping of $5 \times 10^{17}\text{ cm}^{-3}$ and an unintentional intrinsic doping of $1 \times 10^{17}\text{ cm}^{-3}$, which are the doping levels we were able to achieve with our equipment during this experiment, this would result in an electric field that spanned around $200\text{--}300\text{ nm}$ of the intrinsic region. Taking this into account, figure 3(a) shows the chosen device design which includes a 40 nm current spreading layer on top of the device (20 nm of gold and 20 nm of palladium) to form the p-contact. This is followed by a 270 nm thick p-GaN region and a 200 nm thick i-GaN region. The rest of the device consists of $1\ \mu\text{m}$ thick n-type GaN. Figure 3(b) shows a sketch of the device after electrical contact processing. The current spreading layer allows for better carrier collection even if the lower electron energies (less than 5 keV) are almost entirely absorbed within it (see figure 4). The p-GaN layer absorbs electron energies around 8 keV , whereas the intrinsic GaN region absorbs electron energies around the ^{63}Ni emission peak (14 keV). Finally, most electrons having energies above 22 keV are absorbed in the n-GaN region and substrate.

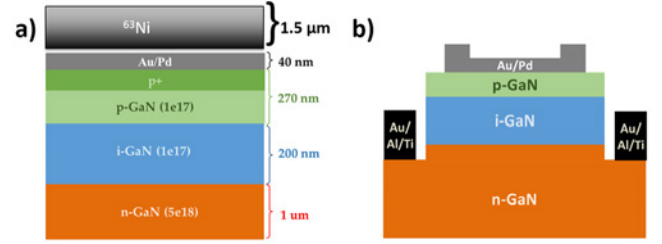


Figure 3. (a) Designed 1 cm^2 area device structure with 200 nm thick intrinsic region and (b) PIN structure with electrical contacts. (not to scale).

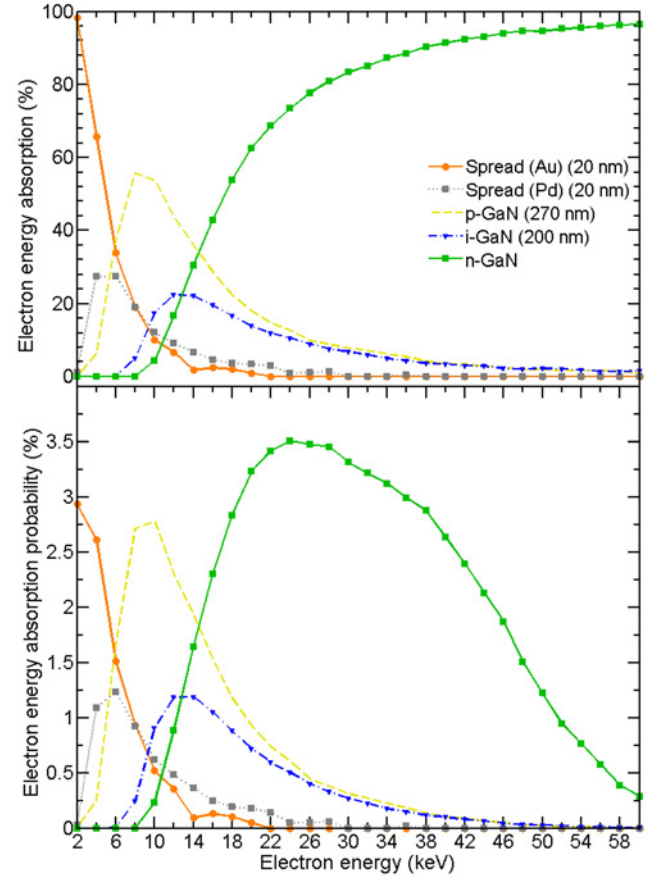


Figure 4. Simulation of the beta particle energy absorption by each layer of the PIN structure (top) and the same energy absorption graph, but now scaled by the probability of beta particle emission (according to the particle energy) from ^{63}Ni material (bottom). Higher energies are less likely to be emitted from ^{63}Ni (and 17 keV is most likely); the bottom graph is designed to visually reflect this.

The power conversion efficiency of a perfect PIN device can be estimated as:

$$PCE(\%) = \eta_{tr} \times \eta_{sp} \times \eta_i \times \eta_{be} \quad (7)$$

where η_{tr} is the amount of energy that is not backscattered from the surface of the device (MC simulations indicate that 29% of the beta particle energy should be backscattered), η_{sp} is the amount of energy that is transmitted through the spreading layer (9% of the beta particle energy is absorbed in the metallic spreading layer, again based on MC simulation), η_i is the amount of electron energy falling within the

i-GaN region (12% of the beta particle energy is absorbed in the i-GaN region, again based on MC simulation as seen in figure 1) and η_{be} is the maximum betavoltaic current efficiency for GaN [13] which is 27%. This leads to a highest possible PCE of around 2.09%.

3.2. Material growth

3.2.1. GaN epitaxy. All the PIN structures were grown at 1030 °C using a T-shaped MOVPE reactor under a pressure of 100 Torr and a V/III ratio of 8000. Trimethylgallium and ammonia were used as precursors for gallium and nitrogen, respectively. SiH₄ and CP₂Mg were used as n-type and p-type dopants, respectively. The growths were performed on 2" sapphire wafers, starting with 1.8 μm thick buffer of intrinsic GaN. The PIN structures were structurally and morphologically characterized with high resolution x-ray diffraction, scanning electron microscope (SEM) and atomic force microscope. The dopant concentrations and their profiles were characterized by Hall effect measurements and secondary ion mass spectroscopy (SIMS) analysis, respectively.

3.2.2. ⁶³Ni deposition. ⁶³Ni was synthesized using neutron and gamma ray bombardment of a ⁶²Ni target followed by an acid dissolution and radiochemical separation in order to obtain ⁶³NiCl₂ radioactive salt. A modified Watts bath was then prepared using ⁶³NiCl₂, H₂O, Na₂SO₄ and H₃BO₃. The ⁶³Ni material was then electrodeposited onto the two sides of a piece of copper foil approximately 1 cm² in surface area with 140 μm thick copper foil, which absorbed all energy that was emitted away from the devices, and using a Pt anode (see figure 5). The deposition yield was approximately 80% leading to 2.4 GBq of activity deposited on the two facets of the copper foil for each source. Assuming a 17keV average beta particle energy, this equates to approximately 6.545 μW of energy emitted (i.e. 3.27 μW emitted from each side of the source).

3.3. Device processing

Three metallic patterns were defined by lift-off using contact photolithography. A thin spreading bilayer of palladium and gold (20 nm / 20 nm) was first deposited as a p-contact on the GaN p + type top layer, over an area of 8 × 8 mm². A contact pad, made of palladium and gold bilayer (20 nm / 200 nm), was subsequently deposited on the side of this spreading layer to allow for wire bonding. The mesa was then dry etched, to a depth of 1 μm, so as to reach the n-type layer. This step was achieved using BCl₃/Cl₂/N₂ inductively coupled plasma reactive-ion etching (RIE), through a SiO₂ mask. The n-contact consisted of titanium / aluminum / gold (10 nm / 30 nm / 300 nm) deposition. To ensure good ohmic contacts, the diodes were subsequently rapid thermal annealed under N₂ atmosphere. A photograph of a fabricated device is shown in figure 6(a). The final steps involved dicing the diodes, mounting on specific holders and wire bonding (see figure 6(b)).

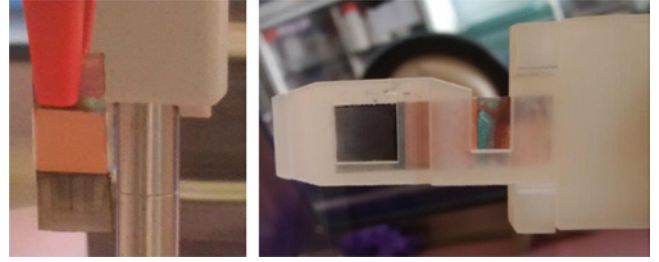


Figure 5. Photographs of a ⁶³Ni layer electrodeposited on a copper foil (left) and mounted in the holder (right).

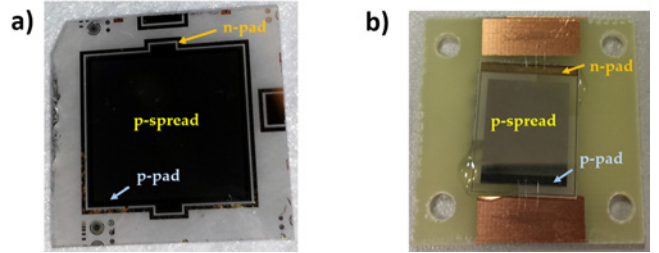


Figure 6. Photographs of (a) a processed device, and (b) a device mounted on a printed circuit board and wire bonded.

3.4. Packaging

In order to facilitate radioactive ⁶³Ni testing within a confined glovebox, a 3D printed sample holder was developed (figure 7). This holder offered the options of both reusability and fine tuneability of the device/source distance using a manual screw mechanism (as seen in figure 7(b)). Notice here that the ⁶³Ni holder can be slid in and out of the testing box via the tray (figure 7(c), top right). It can be seen from figure 7 that each testing box was conceived to house two betavoltaic devices forming a sandwich around the ⁶³Ni source. There is also a turnkey screw mechanism which allows us to vary the source/betavoltaic distance, and thus the power, delivered to the devices. A dagger insertion mechanism provides for easy loading/extraction of both the devices and the ⁶³Ni source, while preventing damage to the wire bonding upon loading. The testing box is equipped with 8 electrical connectors (4 per device) allowing the use of the 4-point probe method for I–V measurements.

4. Results

A total of nine 1 × 1 cm², GaN-based PIN devices and three ⁶³Ni sources were fabricated. Hall measurements revealed p-type and n-type doping levels of around 1 × 10¹⁷ cm⁻³ and 5 × 10¹⁸ cm⁻³, respectively. SIMS revealed the doping depth profiles to have relatively abrupt steps at the interfaces. The PIN devices exhibited a turn-on voltage of around 3.5V and a leakage current on the order of 3–70 μA under a bias voltage of –5V (this current was relatively high because of the comparatively large size of the device). A typical I–V plot of these devices is shown in figure 8.

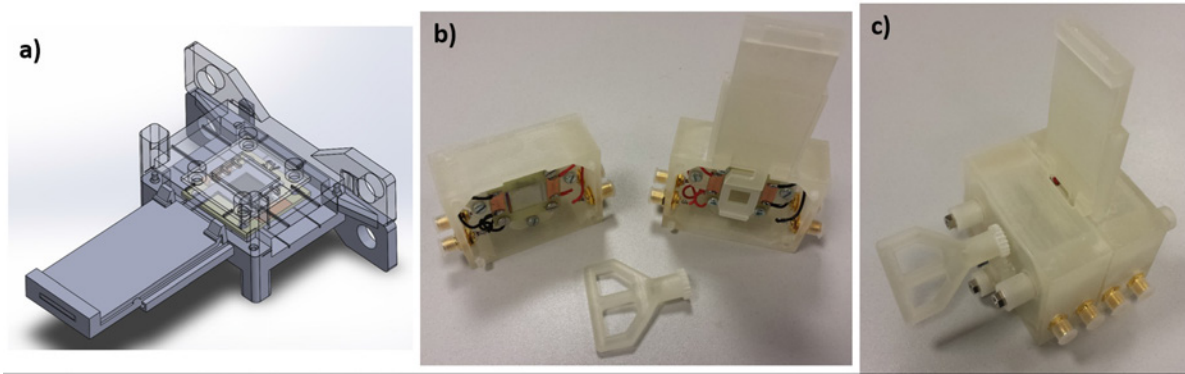


Figure 7. (a) Schematic and photographs of (b) open and (c) closed testing box, with turnkey screw mechanism for varying the betavoltaic to ^{63}Ni source distance.

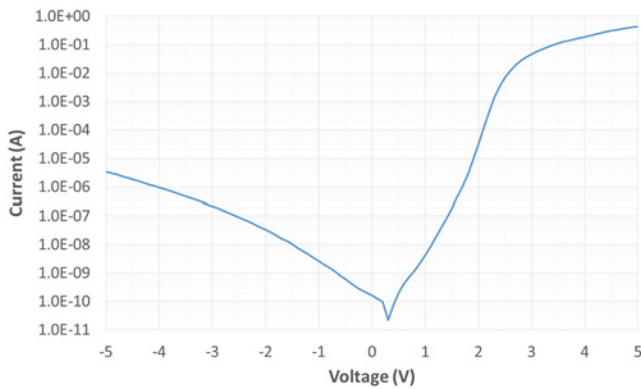


Figure 8. Typical I–V plot of the fabricated PIN devices.

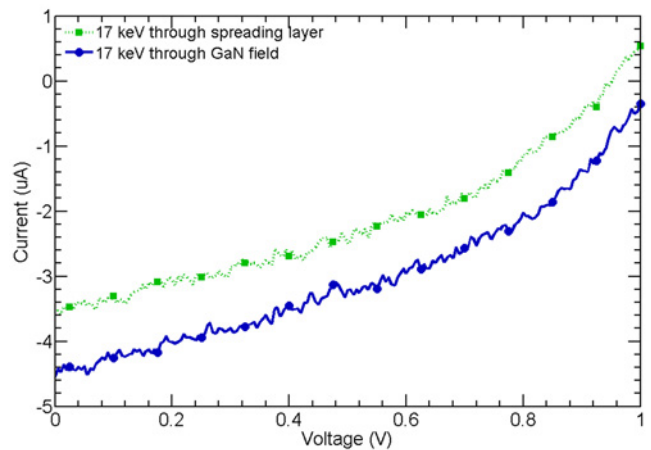


Figure 10. e -beam generated current under $80\ \mu\text{W}$ of irradiation, both through the current spreading layer and directly on the p-GaN field.

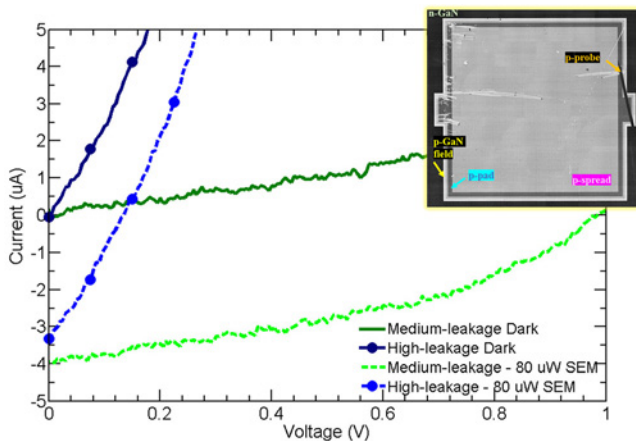


Figure 9. Dark and electron beam exposed IV measurements for two of the devices recorded with a 17 keV beam energy and an $80\ \mu\text{W}$ power. Inset: typical EBIC image, showing consistent current generation throughout the device.

4.1. Electron beam simulation

Before experimenting with actual ^{63}Ni , some preliminary experiments were performed in an SEM using an $80\ \mu\text{W}$ beam power and a 17 keV accelerating voltage (so as to simulate the typical ^{63}Ni beta particle energy). Figure 9 shows both the dark and electron beam IV measurements for two of the devices, which are typical of the devices having high

and medium current leakage, respectively. For both of them, the short-circuit electron beam induced currents (EBIC) are similar and approximately equal to $3.5\text{--}4\ \mu\text{A}$, whereas the open circuit voltages (V_{oc}) are quite different and equal to 150 mV and 1V for the devices having high and medium current leakage, respectively. The inset depicts a typical EBIC image recorded during these experiments, showing a very uniform carrier collection efficiency and thus beta-current generation throughout the entire device. Since the EBIC signal is proportional to the generated current, the EBIC images did not vary significantly between the different devices.

Finally, figure 10 shows the collected current under $80\ \mu\text{W}$ of e -beam irradiation, both through the metallic current spreading contact layer (green line) and directly on the p-GaN field (without any metallization, blue line). The difference between the two curves can be attributed to the absorption of the impinging electrons in the metallic current spreading contact layer or backscattering at a higher amount, which leads to less generated electron-hole pairs in the PIN junction. Thus, the beam current losses in the metallic layer lead to a decrease by around 21% of both the short circuit current and open circuit voltage.

Table 1. Betacurrent experimental measurements for all four devices and with three different ^{63}Ni sources.

Device leakage	Distance to source	$I_{sc}(\text{nA})/V_{oc}(\text{mV})$		
		Box #1	Box #2	Box #3
Medium	5 mm	1.4/800	N/A	1.25/780
High	5 mm	0.95/53	1.35/65	1.1/57
High	0.5 mm	3.1/~0	3/~0	N/A

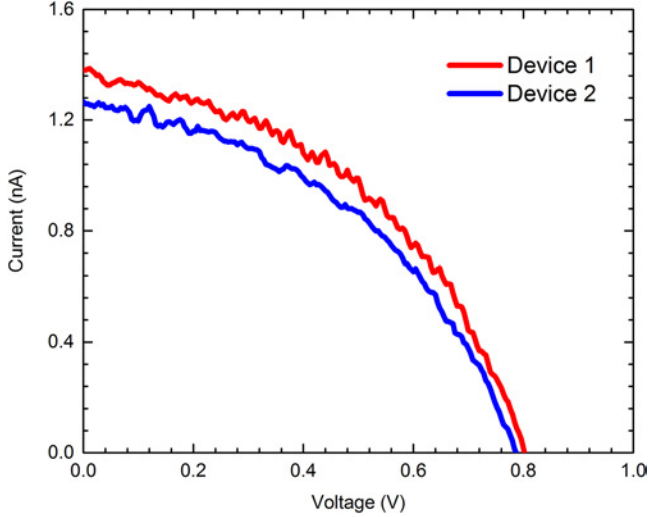


Figure 11. Current-voltage measurements recorded in two medium leakage current PIN devices placed at 5 mm away from the ^{63}Ni source.

4.2. ^{63}Ni experimental data

Among the nine fabricated devices, two were damaged during the mounting in the testing boxes. Among the seven devices that were left, two of them were placed closer to the ^{63}Ni source (around 0.5 mm gap) and the other five were placed at around 5 mm from the ^{63}Ni source (wire bonding prevented closer positioning). Table 1 summarizes the results obtained for the different devices in terms of short circuit current (I_{sc}) and V_{oc} . For all of the devices, the results weakly depended on the box in which the PIN device, and thus ^{63}Ni source, was mounted. It is clear that both the distance to the ^{63}Ni source and the current leakage value affected the performance of the device. As seen in the previous subsection, I_{sc} is only slightly lower for the high leakage current devices (average I_{sc} of 1.15 ± 0.2 nA) than for the medium leakage current devices (average I_{sc} of 1.4 ± 0.2 nA), whereas, a one order of magnitude lower V_{oc} was expected (see figure 11).

Additionally, the I_{sc} for devices placed closer to the ^{63}Ni source (3.05 ± 0.1 nA) is much higher than that obtained for devices positioned 4 mm (9 times) further away. The beta particles counted versus absorber thickness (air in this case), can be estimated by $N(x) = N_0 \times e^{-(\mu_B \times \rho \times x)}$ where N_0 is the initial beta particles counted (at zero absorber thickness), μ_B is the beta absorption coefficient (which is $2071.16 \text{ cm}^2 \text{ g}^{-1}$ for air) and ρ is the density of the absorber ($1.205 \times 10^{-3} \text{ g cm}^{-3}$ for air). This predicts losses of 12 and 68%, respectively, for

Table 2. Mounting dependence of the device performances.

Device mounting	I_{sc} (nA)	V_{oc} (V)	P (nW)	PCE (%)
1 device	1.4	0.79	0.52	0.016
2 in series ^a	1.4	1.58	1.04	0.016
2 in series closer to the source ^b	3	1.58	2.23	0.034

^a Deduced from experiments led on the single device and extrapolated to two devices mounted in series

^b Deduced from experiments led on the single device and extrapolated to two devices mounted in series and placed as close as possible to the source.

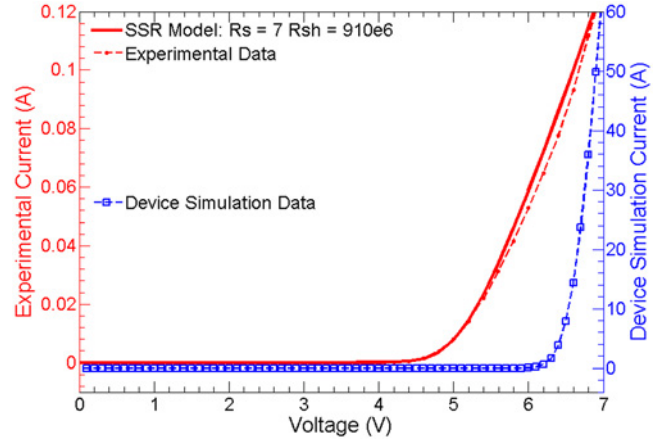


Figure 12. Simulated versus experimental, dark IV curves with two 1 cm^2 PIN devices mounted in series.

gaps of 0.5 and 4.5 mm. Accordingly, an I_{sc} of 3.05 nA for a device placed 0.5 mm from the source should drop to 0.98 nA for a device 4.5 mm away from the source. This is in very good agreement with the measured value of 1.15 ± 0.2 nA.

Particularly noteworthy are the two devices with medium leakage current, which had an I_{sc} of 1.4 ± 0.2 nA, a V_{oc} of 0.79 ± 0.01 V and a fill factor (FF) of 47% (see figure 11), corresponding to a generated power ($P = V_{oc} \times I_{sc} \times FF$) of 0.52 ± 0.08 nW and leading to a PCE of 0.016%. As shown in table 2, the generated power can be easily doubled by connecting the two devices in series (i.e. placing them on either side of the ^{63}Ni source). This leads to a device with a generated power of 1.04 ± 0.1 nW with the same PCE. Furthermore, if the two devices in series are placed closer to the source this leads to an I_{sc} of 3 nA, and the generated power and PCE can be increased to 2.23 nW and 0.034%, respectively.

4.3. Model comparison

The model prepared in section 2 can now be used to compare the predicted device performance with these experimental values. The series device described at the end of the previous subsection (in which devices are positioned in proximity to each side of the ^{63}Ni source) was adopted for modeling. Figure 12 shows both the experimental and simulated (both ideal and SSR models) dark current-voltage curves for this device. The SSR model, with 7Ω and $910 \text{ M}\Omega$ as series and shunt resistance,

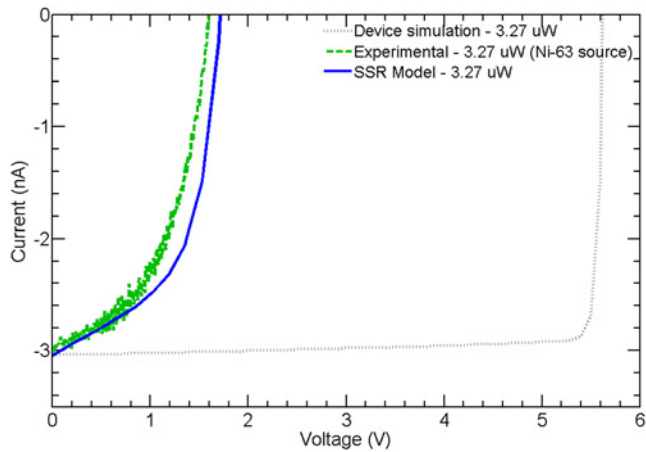


Figure 13. Simulated versus experimental, IV curves for irradiation with a $6.545 \mu\text{W}$ ^{63}Ni beta source ($3.27 \mu\text{W}$ each PIN) and two 1 cm^2 PIN devices mounted in series.

Table 3. Betavoltaic device performance under a $6.545 \mu\text{W}$ ^{63}Ni source and two 1 cm^2 PIN devices mounted in series.

	^{63}Ni model		Exp. data
	Ideal device	SSR model	
I_{sc} (nA)	3.03	3.03	3
V_{oc} (V)	5.6	1.7	1.6
FF (%)	90.9	53.6	46.9
P (nW)	15.42	2.76	2.23
P_D ($\mu\text{W cm}^{-3}$)	68.45	12.25	9.9
PCE (%)	0.23	0.042	0.034

respectively, and an ideality of 3.6, fits the experimental results well. Similarly, figure 13 shows the IV curves under ^{63}Ni irradiation in order to highlight the betacurrents. The green dashed curve is based on the experimental results under ^{63}Ni irradiation ($6.545 \mu\text{W}$ total). The solid blue line shows the SSR model predictions, and the dashed gray line shows the results directly from the ideal. Again, the SSR is in very good agreement with the experimental results, with only a minor variation in the V_{oc} expectations (though still within 0.1 V).

Table 3 shows these results more quantitatively. The ideal device model predicts a generated power of $68.45 \mu\text{W cm}^{-3}$ with a $6.545 \mu\text{W}$ ^{63}Ni input. After adding the SSR model we can see that this drops to $12.25 \mu\text{W cm}^{-3}$, due to a large decrease of both V_{oc} and FF. This is rather close to the experimental results, (which shows $9.9 \mu\text{W cm}^{-3}$), the difference being mostly due to the smaller FF.

5. Conclusion

This paper described the design, fabrication and experimental testing of 1 cm^2 GaN/ ^{63}Ni based betavoltaic batteries and a versatile testing box which allowed for reusability and tuning of the device/source distance. The optimal devices constructed in these experiments achieved an output power of 0.52 nW , which could likely be extended to 1.04 nW if the boxes are run as-designed in series configuration. We


additionally feel a simple reduction of the sample/source gap should allow 2.23 nW output, however. It was proposed that the efficiency of the experimental device was limited predominantly due to the relatively thick p-GaN region (270 nm) and current spreading layers (40 nm), combined with a relatively thin i-GaN region (200 nm) having excessive residual doping. These issues can be improved in the future by optimizing the active layer thicknesses, replacing the i-GaN with dilute B GaN alloy (which allows a several order of magnitude in resistivity [14, 15]), and decreasing the thickness of the current spreading layer down to 20 nm or using interdigitated electrodes.

The paper also presented the development of a ^{63}Ni beta-voltaic simulation model that can be quickly and easily generated with standard Monte Carlo simulation software (such as CASINO) but can still provide high-quality and accurate results that match well with literature. This model was also combined with the device and SSR models, and gave a very good fit with the experimental data.

Acknowledgments

This work was supported by the Agence Nationale de la Recherche of France as part of the BATGAN project (ANR-11-BS09-0038).

ORCID iDs

J P Salvestrini  <https://orcid.org/0000-0002-0482-1178>

References

- [1] Ulmen B, Desai P D, Moghaddam S, Miley G H and Masel R I 2009 Development of diode junction nuclear battery using Ni-63 *J. Radioanal. Nucl. Chem.* **282** 601–4
- [2] Kuruoglu N, Ozdemir O and Bozkurt K 2017 Betavoltaic study of a GaN p-i-n structure grown by metal-organic vapour phase epitaxy with a Ni-63 source *Thin Solid Films* **636** 746–50
- [3] Cheng Z J, San H S, Feng Z H, Liu B and Chen X Y 2011 High open-circuit voltage betavoltaic cell based on GaN pin homojunction *Electron. Lett.* **47** 720–1
- [4] Cheng Z, Chen X, San H, Feng Z and Liu B 2012 A high open-circuit voltage gallium nitride betavoltaic microbattery *J. Micromech. Microeng.* **22** 074011
- [5] Cheng Z-J, San H-S, Chen X-Y, Liu B and Feng Z-H 2011 Demonstration of a high open-circuit voltage GaN betavoltaic microbattery *Chin. Phys. Lett.* **28** 078401
- [6] San H, Yao S, Wang X, Cheng Z and Chen X 2013 Design and simulation of gan based schottky betavoltaic nuclear microbattery *Appl. Radiat. Isot.* **80** 17–22
- [7] Chandrashekar M, Thomas C, Li H, Spencer M and Lal A 2006 Demonstration of a 4H SiC betavoltaic cell *Appl. Phys. Lett.* **88**
- [8] Gao H, Luo S, Zhang H, Wang H and Fu Z 2013 Demonstration, radiation tolerance and design on a betavoltaic micropower *Energy* **51** 116–22
- [9] Wang G, Hu R, Wei H, Zhang H, Yang Y, Xiong X, Liu G and Luo S 2010 The effect of temperature changes on electrical performance of the betavoltaic cell *Appl. Radiat. Isot.* **68** 2214–7

- [10] Munson C, Arif M, Streque J, Belahsene S, Martinez A, Ramdane A, El Gmili Y, Salvestrini J, Voss P and Ougazzaden A 2015 Model of Ni-63 battery with realistic PIN structure *J. Appl. Phys.* **118** 105101
- [11] Tang X, Liu Y, Ding D and Chen D 2012 Optimization design of gan betavoltaic microbattery *Sci. China Technol. Sci.* **55** 659–64
- [12] Honsberg C, Doolittle W, Allen M and Wang C 2005 GaN betavoltaic energy converters *Conf. Record of the Thirty-First IEEE Photovoltaics Specialists Conf.* pp 102–5 (IEEE Electron Devices Soc IEEE 2005 31st IEEE Photovoltaic Specialists Conf. (Lake Buena Vista, FL, 03–07, January 2005))
- [13] Olsen L 1993 Review of betavoltaic energy conversion *NASA Conf. Publication* p 256
- [14] Srour H, Salvestrini J, Ahaitouf A, Gautier S, Moudakir T, Assouar B, Abarkan M, Hamady S and Ougazzaden A 2011 Solar blind metal-semiconductor-metal ultraviolet photodetectors using quasi-alloy of B GaN/GaN superlattices *Appl. Phys. Lett.* **99** 221101
- [15] Ravindran V, Boucherit M, Soltani A, Gautier S, Moudakir T, Dickerson J, Voss P, di Forte-Poisson M-A, De Jaeger J-C and Ougazzaden A 2012 Dual-purpose B GaN layers on performance of nitride-based high electron mobility transistors *Appl. Phys. Lett.* **100** 243503